Critical heat flux as a mass flux dependent local or global phenomenon: Theoretical analysis and experimental confirmation

Originally published:

April 2018

International Journal of Thermal Sciences 130(2018), 200-207

DOI: https://doi.org/10.1016/j.ijthermalsci.2018.04.040

Critical heat flux as a mass flux dependent local or global phenomenon: Theoretical analysis and experimental confirmation

Wei Ding[1], Thomas Geißler[1], Eckhard Krepper[1], Uwe Hampel[1,2]*

[1] Institute of Fluid Dynamics, Helmholtz-Zentrum Dresden-Rossendorf, Dresden, Germany

[2] AREVA Endowed Chair of Imaging Techniques in Energy and Process Engineering, Technische Universität Dresden, Germany

Abstract

In this article, we report on a theoretical analysis and experimental investigations on critical heat flux (CHF) in subcooled flow boiling. Commonly, CHF is considered as a local phenomenon. A validated CHF- concept recently developed in our group indicated that CHF may be initiated in two different ways, that is, locally and globally. We designed and conducted an experiment to verify this hypothesis. The experimental results agree well with the expectations from our CHF- modelling and confirm the two mechanisms. Following that, we continued to clarify the role of different parameters, such as channel orientation, channel length and hydraulic diameter. The new concept of CHF is useful to explain and predict CHF at conditions of low pressure and low fluid velocity.

Keywords: boiling, critical heat flux, initiation mechanisms

1. Introduction

Subcooled flow boiling is one of the most efficient ways to transfer heat, as it combines the uptake of latent heat by bubbles, convective heat transfer via bubble motion and an effective mixing in the thermal boundary layers. However, when the heat flux reaches a critical value, the so-called Critical Heat Flux (CHF), nucleate boiling turns into film boiling. There, parts of the heater surface become irreversibly covered by a thin vapour blanket, which lowers the heat transfer drastically [1] (Figure 1). In power-controlled systems this may jeopardizes the safety as it can potentially lead to a meltdown of the heater. Because of this, the transition from nucleate to film boiling at CHF is still a topic of intense scientific investigation. Though many experimental studies and mechanistic models do exist, a comprehensive understanding of CHF has not yet been achieved. One difficulty comes from the fact, that an optical observation of critical heat flux on metallic heater surfaces is problematic, as the heavy pre-CHF boiling makes the heat transfer fluid opaque and further harsh pressure and temperature conditions hamper the application of measurement techniques.

From many experimental studies it is known that a number of system parameters, such as channel orientation, channel length and hydraulic diameter have a different influence on the CHF under high and low mass flux in flow boiling. However, mechanistic models [2-5] do not consider such effects. In our opinion, the reason for that is that present mechanistic models do consider CHF as a local phenomenon. Our recent analyses, however, indicate that CHF may occur in two different ways, namely in a local and a global one, which should be dependent on the system's mass flux. Local occurrence is happening at low mass flux while at high mass flux CHF appears globally. In this article, we report on a theoretical and experimental study to clarify this issue. Before that, we will firstly give a brief introduction of common knowledge and recent findings in the field.

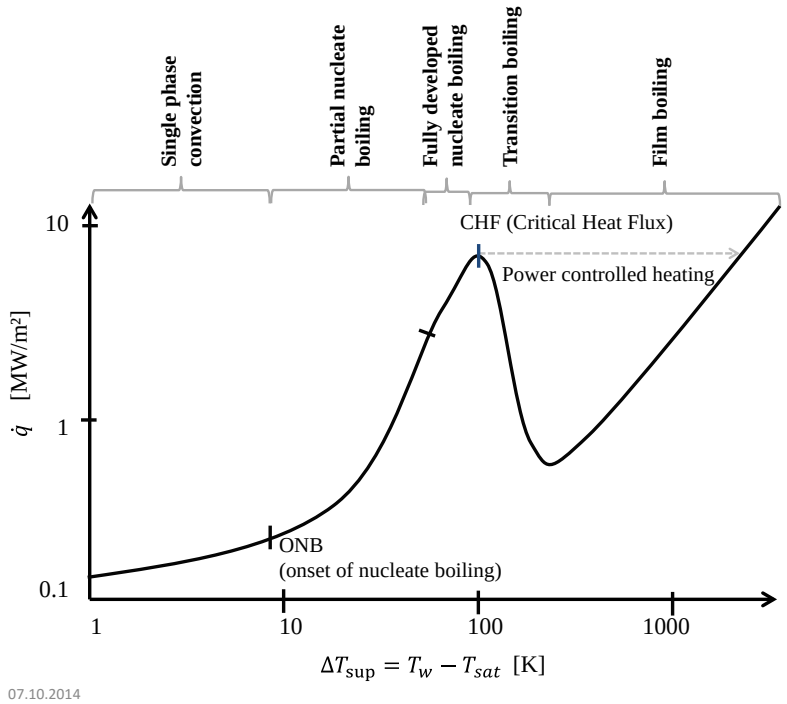

Figure 1: Exemplary boiling curve showing the transitions from single-phase convection to film boiling

1.1 Impacts of various parameters on CHF

In 1963, Bergles [6] identified six main system parameters affecting the CHF: pressure (p), liquid subcooling (ΔT_{sub}), mass flux (G, in subcooled flow boiling), channel length (L), hydraulic diameter (D) of channel (in subcooled flow boiling) and channel orientation (ϕ). He reported that the pressure has a rather weak influence on CHF. That is, for forced convective boiling of water CHF increases around 17% when the pressure changes from 0.14 MPa to 0.6 MPa. Vandervort et al. [7] and Celata [8] claimed that the pressure has even no significant effect on CHF when it is below 2.5 MPa. Sakurai and Shiotsu [9] did experiments to investigate the impact of subcooling on CHF. They found a linear relationship between CHF and subcooling in the entire subcooling region up to saturation. They concluded that the CHF increases with an increase of subcooling in horizontal and vertical pool boiling. Gunther [10] found for flow boiling of water in a rectangular section that CHF also has a linear relationship with subcooling. Bergles found a similar effect but only at relatively high subcooling. Celata and Mariani [2] conducted experiments to study the impact of mass flux on CHF. They indicated that high mass flux could lead to higher CHF, which was widely agreed by others [11-13]. Bergles experimentally observed an impact of the pipe diameter (D) on CHF. He stated that CHF increases with decreasing D. However, this effect becomes less significant for hydraulic diameters above 5 mm. Nariai et al. [3], and Nariai and Inasaka [4] conducted experiments to investigate the effect of the channel length (L) and channel diameter (D) on CHF. They found that at high mass flux, CHF increases when both channel diameter and length decrease. However, at low mass flux, both effects become insignificant for sufficiently high values of L and D. They also found that CHF values are higher at high mass flux and at low mass flux with small L and D. Buoyancy and channel orientation also influence CHF. Pappell et al. [5] demonstrated in experiments with liquid nitrogen in a 12.5 mm diameter tube that buoyancy only plays a role for low mass flux. Celata and Mariani [2] found that the channel orientation plays a role only when mass flux is small. They proposed a criterion based on the comparison of the buoyancy to inertia forces basing on the modified Froude number

$$Fr = \frac{G\cos\phi}{\rho_l\left[gD\left(\frac{\rho_l-\rho_g}{\rho_l}\right)\right]^{1/2}}, \quad (1)$$

where G is the mass flux, ϕ is the orientation angle, ρ_l and ρ_g are the liquid and vapor density, g is the gravitational acceleration and D is tube diameter. They concluded that the effects due to orientation only appear when the modified Froude number is smaller than 5. While the dependency of CHF on the above parameters is well recognized, the mechanisms are still not fully included in the mechanistic models of CHF.

1.2 Mechanistic models and correlations

At present, the most popular mechanistic models of CHF can be classified into four categories [2, 13]: the *hydrodynamic instability model*, the *model of critical enthalpy in the bubble layer*, the *model of vapor removal limit and near-wall bubble crowding model*, and the *liquid sublayer dryout model* (Figure 2). Kutateladze [14] and other researchers [15, 16] hypothesized that CHF of saturated horizontal pool boiling is a purely hydrodynamic phenomenon and that it is triggered by a destruction of the stability of the two-phase flow occurring close to the heated surface (Figure 2a). In 1966, Ivey and Morris [17] further extended this model for subcooled boiling. The '*model of critical enthalpy in the bubble layer*' was proposed by Tong et al. [18]. They considered that a bubbly layer near the heater surface could trap the liquid in between. CHF is reached when this liquid layer attains a certain limiting enthalpy (Figure 2b). The '*bubble crowding model'* was proposed by Hebel et al. [19] who considered the limit of the turbulent interchange between the bubbly layer and the bulk of the liquid and inferred that crowding of the bubbles prevents the liquid access to the heater wall (Figure 2c). Weisman and Pei [20] further quantified this model by the assumption that CHF occurs when the volume fraction of vapor in this bubbly layer exceeds a critical volume fraction of 82%. This definition is based on their experimental observations. The '*liquid sublayer dryout model*' was proposed by Katto and Yokaya [21] and further developed by Haramura and Katto [22], Lee and Mudawar [23] and Celata et al [24]. This model assumes that a liquid film forms near the heater wall because of a Helmholtz instability (Figure 2d) and CHF is reached when the heater can provide the necessary latent heat to completely evaporate the liquid entering the film between the liquid sublayer and wall. All these models can to some degree achieve agreement with experimental data, but they contain quite a few empirical constants or empirical correlations [13]. As many of these model concepts and correlations are for subcooling boiling at high pressure and high velocity (HPHV) they typically produce larger disagreement at low pressure and low velocity conditions [12]. Moreover, the existing model concepts do mostly not contain the dependencies on the above-mentioned system parameters, such as channel orientations, channel length and hydraulic diameter on CHF at low and high mass flux.

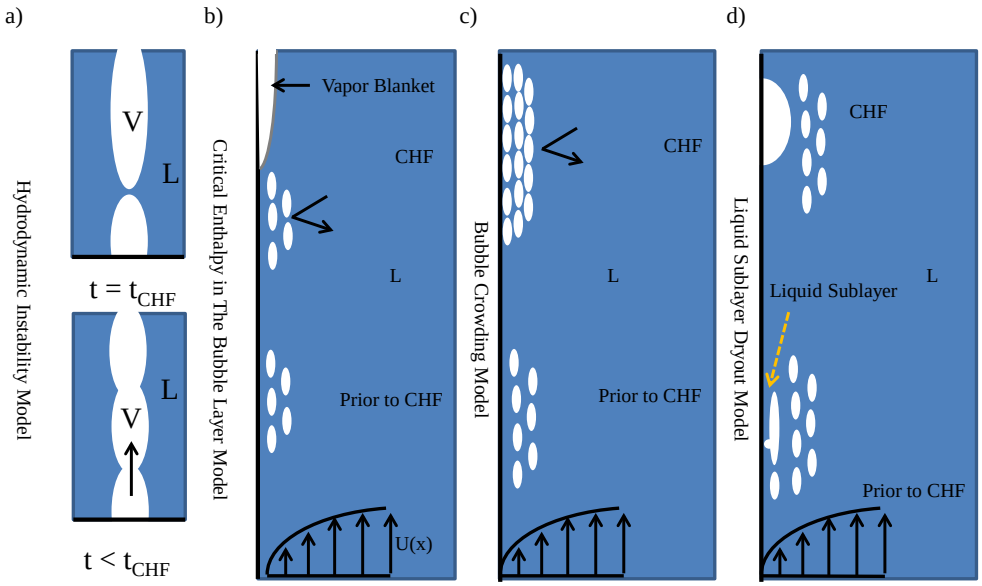

Figure 2: CHF mechanisms according to a) the hydrodynamic instability model, b) the model of critical enthalpy in the bubble layer, c) the bubble crowding model, d) the liquid sublayer dryout model. V stands for vapor, L stands for liquid and the turning arrows indicate partial blockage of liquid supply to the wall.

2. CHF- Concept and Model

Recently, we developed a model of prior critical heat flux (CHF-) from the models of bubble dynamics at nucleate boiling [25]. It holds for pool boiling and forced convective boiling and incorporates a mutual effect model and a shear stress model. The model is capable to explain the initiation mechanisms of the boiling crisis and impacts of different variables. In the following section, the main idea of this CHF- concept will be briefly introduced.

The bubble growth at a small cavity in the heater wall is considered as a stable and repeatable process which consists of activation, growth, departure and reactivation with certain durations (Figure 3). Most important periods are the total growth period t_g and the waiting time t_w between bubble departure and new activation. The total transferred heat Q_b during bubble growth consists of three parts: heat flowing from the wall into the bubble via evaporation ($Q_{b,w}$), heat flowing from the superheated liquid near the wall into the bubble ($Q_{b,s}$) and condensation heat transfer to the bulk liquid at the upper part of the bubble ($Q_{b,c}$). That is, the heat input to the bubble comes from two sources: the wall and the thermal boundary layer, though we cannot say for the moment, how the share is quantitatively. After bubble departure, a waiting time is required to regenerate the nucleus in the cavity and to recover the thermal layer. In this time, the quenching heat Q_q is delivered from the wall to the liquid. As during bubble growth the liquid in the vicinity of the bubble has gained the heat $Q_{b,c}$ and lost the heat $Q_{b,s}$, we may assume that $Q_q = Q_{b,s} - Q_{b,c}$. The heat balance can then be written as

$$Q_{b,w} + Q_q = Q_{b,w} + Q_{b,s} + Q_{b,c} = Q_b = \frac{4}{3}\pi {r_d}^3 \rho_g h_{fg}, \qquad (2)$$

with h_{fg} being the latent heat of the fluid.

Then we define the projective area $A_b = \pi r_d^{\,2}$ of a fully developed bubble with departure radius r_d as the apparent heat transfer area for boiling heat transfer per single bubble. The heat flux in this area during bubble growth is then

$$\dot{q} = \frac{Q_{b,w} + Q_q}{\pi r_d^{\,2}(t_g + t_c + t_w)} = \frac{Q_b}{\pi r_d^{\,2}(t_g + t_c + t_w)} = \frac{(\frac{4}{3}\pi r_d^{\,3}\rho_g h_{fg})}{\pi r_d^{\,2}(t_g + t_c + t_w)}, \tag{3}$$

where t_c is the condensation time which is only for the case where the bubble will activate, grow, shrink and collapse on the cavity in high subcooling as shown in Figure 3 c). For saturation or low subcooling conditions we may set $t_c = 0$.

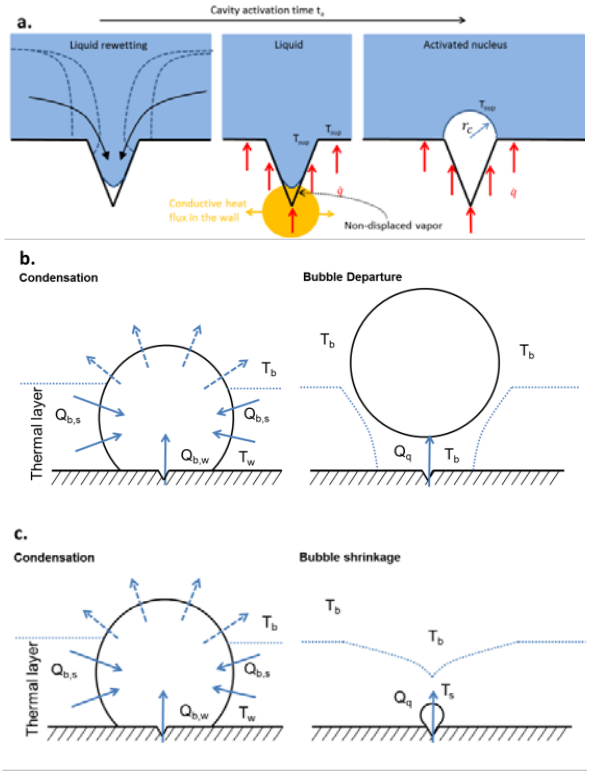

Figure 3: a) Cavity activation and heat transport during and after bubble growth: b) bubble departure in the low subcooling case and c) bubble shrinkage in the high subcooling case in horizontal pool boiling [25].

During rewetting the replenishing liquid partially displaces the vapor in the cavity [26, 27]. Before the bubble cycle closes it takes a time period t_a (cavity activation time) to form a new vapor nucleus with critical radius r_c on the mouth of cavity, which is the activation condition. The formation of this vapor nucleus requires superheating of liquid in the cavity to overcome the high pressure in the nucleus. In the upper part of the cavity liquid touches the wall and we may assume that heating up this liquid has the same time scale as above the wall outside the cavity. In the lower part of the cavity there is vapor in direct contact with the cavity wall, which gives a low heat transfer coefficient. Hence we have a microscopic “film boiling” situation on the bottom of the cavity, which leads to a stronger superheat of the wall there. Conductive heat transfer towards the liquid through the wall material is then the major heat removal mechanism. The higher the heating power the higher becomes the wall superheat at the bottom of the cavity. On the other hand, as the vapor in the lower part of the cavity presents a strong heat transfer resistance, the liquid in the center of the cavity is heated slower than in single

phase conditions and evaporation into the nucleus is delayed. This effect determines the activation time t_a. As the vapor pocket delays the heating of the liquid in the cavity, we can assume that the recovery of the thermal boundary layer (recovery time t_r) occurs faster than the reactivation of the cavity, that is $t_a > t_r$. With increasing heating power or heat flux this situation can change. The wall material at the bottom of the cavity will superheat so much, that reheating of liquid in the cavity is again synchronous with the build-up of the thermal boundary layer outside the cavity, that is, $t_a = t_r$. If the heat flux further increases, the activation time becomes even shorter, the vapor nucleus grows rapidly into the yet not established thermal boundary layer and transfers additional heat to the boundary layer, then $t_a < t_r$. The larger one of t_r and t_a decides the total waiting time, that is, $t_w = max(t_a, t_r)$. For $t_a < t_r$ the situation is unstable, as increasing vapor content in the cavity will further increase cavity wall superheat and further shorten t_a. Eventually the temperature of the cavity wall and the vapor becomes so high, that the rewetting liquid will be directly evaporated on the wall before it flows into the cavity. Then macro film boiling on the wall sets in. As in practice the cavity geometry is generally unknown, it is highly difficult to provide a mechanistic modelling for the heat transfer processes inside the cavity. However, the decisive point is, that $t_a = t_r$ is a significant feature of critical heat flux. As we will derive below, this criterion together with heat flux balances is sufficient to determine the onset of CHF without any further modelling of in-cavity processes. As at this point the system is still marginally stable, we consider the heat flux at this very moment as near critical heat flux CHF-. With Eq. (3) and $t_w = t_a = t_r$ it is given as

$$CHF = \frac{(\frac{4}{3}\pi {r_d}^3 \rho_g h_{fg})}{\pi {r_d}^2 (t_g + t_c + t_r)}. \quad (4)$$

According to Zhao [28], under constant heat flux, the thermal layer recovery time is derived as

$$t_r = \left[\frac{\pi k_l}{2\dot{q}}\right]^2 \frac{(T_w - T_b)^2}{\pi \alpha_l}, \quad (5)$$

where $\dot{q}$ is the feeding heat flux, T_w is the wall temperature, T_b is bulk temperature, k_l is the liquid thermal conductivity and α_l is the liquid thermal diffusivity. As stated earlier, the bubble growth rate in the inertia controlled period is much higher than for thermal diffusion. As inertial growth is quite fast, we may omit this period in further calculations and just consider the thermal diffusion controlled growth, giving $t_g = \left(\frac{r_d}{B}\right)^2$ from Mikic [29], where B is a factor for evaporation written as $B = \left(\frac{12}{\pi}\alpha_l\right)^{\frac{1}{2}} \frac{\rho_l c_{pl} (T_w - T_{sat})}{\rho_g h_{fg}}$. Thereby, T_{sat} is saturation temperature and c_{pl} is liquid specific heat capacity. In the high subcooling case, we may assume that the condensation on the bubble also follows the rule of growth but opposite to evaporation with a factor B_c with subcooling $T_b - T_{sat}$. Then the condensation time t_c can be calculated with t_g as

$$t_c = \left(\frac{r_d}{B_c}\right)^2 = t_g \frac{(T_w - T_{sat})^2}{(T_b - T_{sat})^2}. \quad (6)$$

Note, that we have readily assumed that the gas in the bubble and the condensed liquid around it is always at saturation temperature (Figure 3c). The same holds for the rewetting liquid in low subcooling, as this is a mixture of the liquid surrounding the bubble. To keep notation less complex we will in the following introduce the latent heat $H_s = \rho_g h_{fg}$ and the parameter $X = \left(1 + \frac{\left(T_w - T_{sat}\right)^2}{\left(T_b - T_{sat}\right)^2}\right)$. r_d is the departure radius, which is in some cases dominated by thermal properties and in other cases by the shear stress.

When r_d is dominated by local conditions and thermal properties, the critical departure diameter is defined as

$$r_{d,c} = \frac{2}{3}\left(\frac{1}{2}\cdot\frac{(T_w - T_{sat})}{(T_w - T_b)} + 1\right)\cdot\frac{\left((T_w - T_{sat})\right)}{\left(\frac{(T_{sat} - T_b)}{2}\right)} C^* \sqrt{\left(\sigma/g\Delta\rho\right)} \left(\left(\frac{12}{\pi}\alpha_l\right)^{\frac{1}{2}} Ja^*\right)^n, \quad (7)$$

where $Ja^* = \frac{\rho_l c_{pl}(T_{sat})}{\rho_g h_{fg}}$, $C^* = 1.09e-7$ and $n = 1.7$ for water [30-31]. The calibration process itself is described in [25].

When r_d is dominated by the shear stress, the critical departure diameter is defined as

$$r_s = \frac{C_2 \cdot 2\sigma k_l}{\mu_l h_c u_{max} Pr^{1/3}} = \frac{0.000364 \cdot \left(\frac{D}{D_0}\right)^{0.35}\left(\frac{L}{L_0}\right)^{0.25}\left(\frac{P}{P_0}\right)^{-2.9}\left(\frac{G}{G_0}\right)^{1.15} f(\Delta T_b)}{h_{c,s} u_{max}} \cdot \frac{2\sigma k_l}{\mu_l Pr^{\frac{1}{3}}}, \quad (8)$$

where σ is the surface tension, $u_{max} = \frac{120}{98}\bar{u}$ is the maximum velocity, and $\bar{u}$ is the average velocity in the flow channel. $h_{c,s}$ is heat transfer coefficient for single phase [32] defined via a Dittus-Boelter type equation as

$$h_{c,s} = 0.023\frac{k_l}{D}\left(\frac{DG}{\mu_l}\right)^{0.8}\left(\frac{\mu_l c_{p,l}}{k_l}\right)^{0.4}, \quad (9)$$

D is the diameter of pipe, and G is the mass flux, and μ_l is liquid viscosity.Thereby $f(T_b)$ is a function of the bulk temperature T_b, which is given as

$$f(T_b) = \begin{cases} \left(\frac{\Delta T_{b,0}\,[k]}{\Delta T_b}\cdot\frac{h_{c,s}}{h_{c,s,0}}\right)^{0.25} & \Delta T_b > \; 26\,[K]\cdot\frac{h_{c,s}}{h_{c,s,0}} = 7.32\times10^{-4}[K^2m^2W^{-1}]h_{c,s} \\ 1 & \Delta T_b \leq \; 7.32\times10^{-4}[K^2m^2W^{-1}]h_{c,s} \end{cases} \quad (10)$$

$h_{c,s,0} = 3.55 \times 10^4\ \mathrm{W\,m^{-2}\,K^{-1}}$ is the single phase heat transfer coefficient at the reference point calibrated from Bergles' experiments. In flow boiling the bubble will be inclined as a truncated spherical bubble. We may assume the surface tension force in the wall tangential direction is C_2 times of that in the wall perpendicular direction of a regular spherical bubble. In the original paper, it is found to be $C_2 = 3.64e-4$ for water. CHF usually happens randomly without any schematic order at the downstream part near the end or just at the end of the pipe or channel [33-35]. In our case, for simplification, we consider that CHF always happens at the end of the pipe. The excess bulk temperature measured in the Bergles' case is ΔT_b in the calculation of r_s.

Then Eq. (4) yields

$$CHF = \frac{B^2}{2\cdot min\left(Xr_{d,c}, r_s\right)}\left[\frac{4}{3}H_s - \sqrt{\left(\frac{4}{3}H_s\right)^2 - \frac{X\left(k_l(T_w - T_{sat})\right)^2\pi}{\alpha_l B^2}}\right]. \quad (11)$$

This particular dependency on $Xr_{d,c}$ and r_s leads to the interpretation that CHF may occur as two different phenomena. One is a local CHF when $Xr_{d,c}$ dominates. The CHF- will then be based on local conditions and independent of the void fraction in the bulk. It usually occurs in pool boiling or forced convective boiling with low mass flux. The other is a global CHF when r_s dominates. Because r_s is determined by local shear stress, CHF will be impacted by the void fraction in the bulk, which is dependent on the upstream conditions and also the diameter and length of the channel. It occurs in forced convective boiling with high mass flux. The concept and model was already validated with six different experiments covering different operational conditions such as pressure, mass flux, subcooling, wall surface properties, channel length and diameter and so on in pool and flow boiling process with water [25].

2.1Extension of the CHF- concept

The $r_{d,c}$ in the CHF- model was derived based on the formula of Cole and Rohsenow [36]

$$r_d = \frac{1}{2} C \left(\sigma / g(\rho_l - \rho_g) \right)^{\frac{1}{2}} \left(\rho_f c_{pl} T_{sat} / \rho_g h_{fg} \right)^{1.25} = C \left(\sigma / g(\Delta\rho) \right)^{\frac{1}{2}} (Ja^*)^{1.25} \quad (12)$$

and further considers the mutual effect raised by Kolev in 1994 [37].
The mutual effect can be described as an average fluctuation velocity, which enhances an additional shear stress and leads to earlier bubble departure. It is given as

$$\bar{\bar{V}}' = 2\bar{A}^2 \overline{\tau_g} (\pi N)^{1/2} = 2\bar{A}^2 \overline{\tau_g} \frac{1}{r_{d,c}} \approx \bar{A} = \left(\frac{\pi}{7} \frac{h_{fg} \rho_g \overline{\Delta T_{sup}}}{\rho_l T_{sat}} \right)^{\frac{1}{2}} \propto \left(\frac{\overline{\Delta T_{sup}}}{Ja^*} \right)^{\frac{1}{2}}. \quad (13)$$

As is stated in Eq. (13), $\overline{\Delta T_{sup}}$ and T_{sat} impacts the fluctuation velocity $\bar{\bar{V}}'$ and further the critical departure radius $r_{d,c}$. In our recent analysis [25] we employed the experimental data from Sakashita [30], [31] to derive $r_{d,c}$ for pool boiling. As stated by Sugrue et al. [38], the pressure increase from 1 bar to 5 bar leads to 52% higher saturate temperature but no considerable change of $\overline{\Delta T_{sup}}$. Hence, at that time, we neglected $\overline{\Delta T_{sup}}$ in the derivation of $r_{d,c}$. That is, Eq. (7) comes without $\overline{\Delta T_{sup}}$ while the dependency of $r_{d,c}$ on T_{sat} or Ja^* is given. Comparing Eq. (7) and (12), the impact of Ja^* on the change from r_d to $r_{d,c}$ via $\bar{\bar{V}}'$ can be defined as

$$\frac{r_{d,c}}{r_d} \propto B^{*(1.7-1.25)} = B^{*0.45} \propto Ja^{*0.45}. \quad (14)$$

Now, we would like to extend the model towards low mass flux flow boiling at a constant pressure. According to Chen 1966 [32] the heat transfer coefficient is given as

$$h_c = 0.023 \frac{k_l}{D} \left(\frac{DG(1-\varphi)}{\mu_l} \right)^{0.8} \left(\frac{\mu_l C_{p,l}}{k_l} \right)^{0.4} \cdot F = \frac{\dot{q}}{\overline{\Delta T_{sup}} + \overline{\Delta T_{sub}}}. \quad (15)$$

Here, φ is the weight fraction of vapour and F is a function of the two-phase pressure drop [32]. As h_c depends on $\overline{\Delta T_{sup}}$ and G, we must further consider this dependency.

From Eq. (13) we see, that the impact of $\overline{\Delta T_{sup}}$ on $r_{d,c}$ should be similar to that of $(\frac{1}{Ja^*})$, which is further quantified in Eq. (14)and gives

$$\frac{r_{d,c}}{r_d} \propto \left(\overline{\Delta T_{sup}}\right)^{-0.45}. \quad (16)$$

Because r_d is not a function of $\overline{\Delta T_{sup}}$, this dependency can be simplified to

$$r_{d,c} \propto \left(\overline{\Delta T_{sup}}\right)^{-0.45}. \quad (17)$$

If we have a calibrated reference value $r_{d,c,0}$, Eq. (16) can be rewritten as

$$\frac{r_{d,c}}{r_{d,c,0}} \propto \left(\frac{\overline{\Delta T_{sup}}}{\overline{\Delta T_{sup,0}}}\right)^{-0.45}. \quad (18)$$

If $x = \frac{\overline{\Delta T_{sub}}}{\overline{\Delta T_{sup}}}$, then the Eq. (15) can be rewritten as

$$\overline{\Delta T_{sup}}(1+x) = \frac{\dot{q}}{h_c}. \quad (19)$$

Then for the same heat flux, Eq. (15) yields

$$\frac{r_{d,c}}{r_{d,c,0}} \propto \left(\frac{h_{c,0,i}(1+x_i)}{h_{c,0,0}(1+x_0)}\right)^{0.45}. \quad (20)$$

In order to simplify the calculation, we will further assume that x_i is always approximately equal to x_0 in this low subcooling case.

3. Experiment

An experimental setup has been devised, which allows investigating the boiling heat transfer and local development of CHF. The setup (Figure 4) is a flow loop operated with the refrigerant Octafluorocyclobutane (RC318) (boiling point 25°C at 0.315 MPa pressure, ρ_g= 35.7 kg/m³, ρ_l=1365 kg/m³, c_{pl}=1130 J/(kgK), k_l=0.063 W/(mK), h_{fg} =100,560 J/kg). Due to the lower boiling point compared to water, the experiment facility with RC318 is easier to operate and control. The heated test section is an 80 mm long vertical stainless steel tube (outer diameter 20 mm, thickness 0.3 mm) axially connected to massive copper conductor tubes. The distance between the inlet to the heated section is 450 mm to ensure a fully developed flow. The refrigerant loop comprises a pump for conveying the liquid, two plate heat exchangers for adjusting sub-cooling temperatures and removing the heat, and an expansion vessel for safety reasons in case of an uncontrolled burn-down of the heater. Additional auxiliary systems (refrigerant maintenance pump, vacuum pump, storage vessel) are available for refrigerant handling.

The facility is equipped with an infrared camera (Infratec VarioCam HD) and gold mirrors to measure wall temperatures at the test section with a nearly full 360° angular coverage. The infrared camera has a resolution of 640x480 pixels at a frequency of 60 Hz. A special fast camera-signal based safety shut-down mechanism prevents heater destruction when boiling crisis is reached. The whole facility is combined with a fast X-ray tomography scanner system [39], which has, however, not been used in this study.

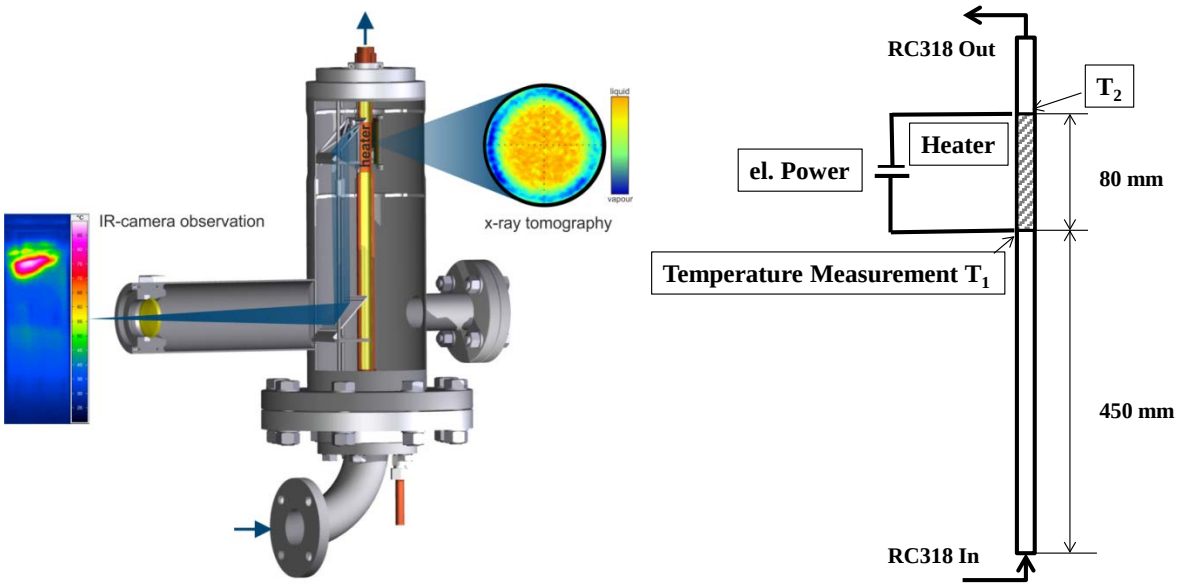

Figure 4: Multi Geometry Critical Heat Flux Observation facility (MORENA).

Experiments were run at different mass fluxes. For each mass flux we started heating at a total rate of 62% of CHF and increased the heating power in 6 to 7 steps with a gradually decreased power increment from 9% to 2.5% of CHF until CHF detection. Before each stepwise power increase, we waited until the wall superheat was in equilibrium, which could be derived from a distributed wall temperature measurement with a Fiber Bragg Grating sensor [40]. The experimental standard deviation in the measured CHF values was determined as 2.4% from multiple tests.

4. Results and Discussion

The CHF- concept [25] requires calibration of the boiling onset, which accounts for the wall material and surface characteristics. The onset is calibrated with the case of G = 990 kg m^{-2} s^{-1} and $\Delta T_{sub,in}$ = 3.3 K. The onset wall superheat is 2.64 K. Though the applied liquid in the experiment is RC318, we found that the value of C_2 in the calculation of r_s is approximately equal to that of water ($C_2 = 3.64e-4$). The model with these two calibrated constants has been further applied to predict the CHF under all conditions.

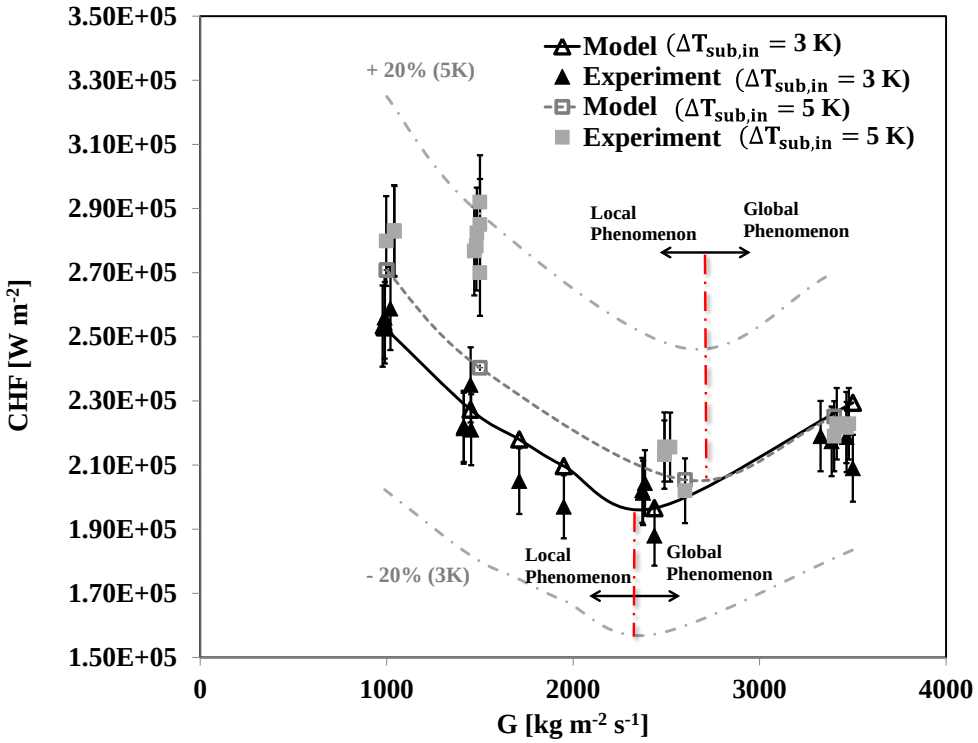

Figure 5: Comparison of experimental and calculated critical heat flux versus mass flux at ~ 3K and ~ 5 K inlet subcooling.

The average error between experiment and model is around 5.3%. As shown in Figure 5, CHF decreases and then increases with an increase of mass flux. The critical mass flux for 3 K subcooling is around 2400 kg m^{-2} s^{-1}. That is, when the mass flux is less than 2400 kg m^{-2} s^{-1}, the CHF is initiated with the mechanism corresponding to $r_{d,c}$, that is, CHF is locally initiated. When the mass flux is larger than 2400 kg m^{-2} s^{-1}, the CHF is initiated with the mechanism corresponding to r_s, which is dependent on the void fraction and local flow pattern. In this case, CHF is globally initiated. Further, with an increase of the subcooling temperature from 3 K to 5 K, the critical mass flux increases from ~2400 kg m^{-2} s^{-1} to ~2800 kg m^{-2} s^{-1}. The experimental results confirm the hypothesis of two initiation mechanisms from the theoretical CHF- concept.

As channel orientation, channel length and hydraulic diameter are known to have an impact on CHF we applied the CHF- concept to explain previous experimental findings qualitatively. At high mass flux the bubble departure is dominated by shear stress (Eq. (8)), no matter, if orientation is vertical or horizontal. But for pool boiling and low mass flux flow boiling, buoyancy plays a role (as modelled by the term $g(\Delta\rho)$ in Eq. (7)). Buoyancy is impacted by the orientation angle. That is, in low mass flux cases, CHF can still depend on orientation angle (Celata and Mariani, [2]). This conclusion holds e.g. for the studies of Papell et al 1966 [5] on the effect of buoyancy at different mass flux conditions. Further we refer to the investigation of the impact of L and D by Nariai and Insaka [4] to assess the role of outlet subcooling. For a similar outlet subcooling and local CHF channel length L and channel diameter D have an effect on CHF via the average heat transfer coefficient (Eqs. (7), (9) and (20)). This impact is, however, not very significant (Figure 6a). But CHF will be significantly impacted by L, D and L/D ratio at high mass flux when CHF is globally initiated, because there CHF is directly dependent on L and D (Eq. (8)). This conclusion agrees well with the experimental finding of Nariai and Insaka in 1992.

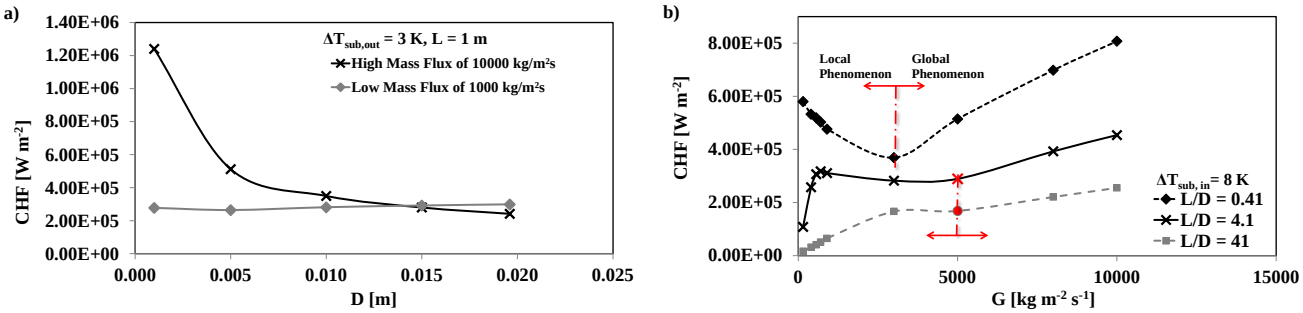

Figure 6: Calculated critical heat flux for a) different pipe diameters (L/D ranges from 50 to 1000) at high and low mass flux and constant outlet subcooling of 3 K and b) different mass flux with different L/D ratio (D = 0.02 m) at constant inlet subcooling of 8 K.

Further we extended our study to consider a larger mass flux range (150 to 10000 kg/(m²s)) for different L/D ratios (Figure 6b). Different to the Figure 6 a), the subcooling at inlet is the condition of modeling in Figure 6 b) As the natural circulation velocity is usually is around 0.1 m/s, we set the lowest mass flux to 150 kg/(m²s). Further we did the CHF calculation with a constant inlet subcooling of 8 K. The simulation results indicate that the impact of mass flux on CHF differs for different L/D ratio. For small L/D ratios an increase of mass flux leads to a decrease of CHF when it is locally initiated. When the L/D ratio becomes intermediate, CHF increases firstly and then decreases until it turns into a global phenomenon. Further when the L/D ratio is large enough, the increase of mass flux will not lead to a decrease of CHF even when it is locally initiated. When CHF is a globally initiated, the CHF always increases with an increase of mass flux.

CHF at low pressure and low velocity (LPLV) conditions is important for nuclear reactors in accident conditions as well as small district heating reactors [12]. Therefore it has been widely investigated for several decades. But it was still not well predicted by the present models or correlations which were made for high pressure and high velocity (HPHV) conditions [41]. Chang et al. [12] conducted an experiment at 1 bar with water at low mass flux in a pipe of L/D = 82. They found that the measured zero-flow CHF (30 – 40 kW/m²) is much lower than the one predicted by an ordinary pooling boiling CHF correlation (~ 1000 kW/m²). They conjectured that the possible CHF mechanisms under LPLV conditions are flooding, churn to annular flow transition, dryout of liquid film in slug flow and dryout of liquid film in annular flow, which leads to an overestimation of the CHF value by the present mechanistic models or correlations generated for HPHV conditions. From this work, we find the missing chain between the CHF at low mass flux conditions and CHF in pool boiling. At smaller L/D ratio, CHF at lowest mass flux becomes larger. We believe that it will approach to the pool boiling CHF value when L/D decreases to a relatively low level. We may further conclude that the overestimated prediction of the CHF at LPLV conditions by common models or correlations may be just because of different CHF initiation mechanisms, which we have now introduced in the CHF- concept.

5. Conclusion

There are two initiation mechanisms of CHF derived from the CHF- concept. One is dependent on the local conditions. In this case, CHF is a local phenomenon. The other is dependent on the void fraction in the bulk that is a global effect from upstream. Then, CHF is a global phenomenon. In this work, these two different mechanisms and phenomena were clearly confirmed by experiments at different mass fluxes and subcooling. The two occurrences of CHF and the corresponding mechanisms explain different impacts of variables such as channel orientation angle, buoyancy and L/D at high and low mass flux, which were already found in earlier investigations. Further it also explains the failure of CHF prediction at low pressure and low velocity (LPLV) conditions with common mechanistic models and correlations.

Further it was found that the impact of mass flux on CHF for the two different phenomena is different. When CHF is local, it CHF decreases with an increase of mass flux at a small L/D ratio. At an intermediate L/D ratio, CHF increases firstly and then decreases with the increase of mass flux. Further it increases with the increase of mass flux at a high L/D ratio. In the high mass flux range, when CHF is a global phenomenon, it increases with

the increase of mass flux, as was already observed by other researchers. The CHF- concept seems to provide the missing modelling link between pool boiling and zero velocity flow boiling.

Acknowledgments

This work is funded by the German Federal Ministry of Economic Affairs and Energy (BMWi) under grant number 1501473C on the basis of a decision by the German Bundestag.

Nomenclature

A	a parameter defined as $\frac{\pi}{7}\frac{h_{fg}\rho_g\overline{\Delta T_{sup}}}{\rho_l T_{sat}}$
A_b	projective area of bubble defined as πr_d^2
B	a parameter defined as $\left(\frac{12}{\pi}\alpha_l\right)^{\frac{1}{2}} Ja$
B^*	a parameter defined as $\left(\frac{12}{\pi}\alpha_l\right)^{\frac{1}{2}} Ja^*$
B_c	a parameter defined as $\left(\frac{12}{\pi}\alpha_l\right)^{\frac{1}{2}} \rho_l c_{pl} \left(T_b - T_{sat}\right)/\rho_g h_{fg}$
c_{pl}	specific heat capacity of liquid
C^*, C_2	constant or parameter
Fr	modified Froude number
D	hydraulic diameter
G	mass flux
g	gravity
H_s	a parameter defined as $\rho_g h_{fg}$
h_c	heat transfer coefficient
$h_{c,s}$	heat transfer coefficient for single liquid phase
h_{fg}	latent heat
Ja	Jakob number
Ja*	modified Jakob number $\rho_l c_{pl} T_{sat}/\rho_g h_{fg}$
k_l	liquid thermal conductivity
L	length of heated wall
N	nucleation site density
n	constant
p	pressure
Pr	Prandt number
$\dot{q}$	heat flux
$\dot{q}_{CHF-}$	critical heat flux
Q	heat of bubble life cycle
Q_b	heat in the bubble
$Q_{b,c}$	heat due to condensation around the bubble
$Q_{b,s}$	heat flowing from superheated liquid surrounding the bubble
$Q_{b,w}$	heat of bubble from wall
Q_q	quenching heat
r	radius
r_c	critical radius on the mouth of cavity
r_d	bubble departure radius

$r_{d,c}$	critical departure radius due to local conditions
r_s	critical departure radius due to shear stress
T_b	bulk temperature
T_w	wall temperature
T_{sat}	saturation temperature
ΔT_{sup}	superheat
$\overline{\Delta \mathrm{T}_{\mathrm{sup}}}$	averaged wall superheat
ΔT_{sub}	subcooling
t	time
t_a	cavity activation time
t_c	bubble condensation time
t_g	bubble growth time
t_r	thermal layer recovery time
t_w	bubble waiting time
τ_g	inertial growth time
$\overline{\overline{V'}}$	average fluctuation velocity
X	a parameter defined as $1+\frac{(T_w-T_{sat})^2}{(T_b-T_{sat})^2}$
x	a parameter defined as $\frac{\overline{\Delta T_{sub}}}{\overline{\Delta T_{sup}}}$
α_l	liquid thermal diffusivity
ϕ	orientation angle
σ	surface tension
μ	viscosityof liquid
ρ_g	density of vapor
ρ_l	density of liquid
$\Delta\rho$	density difference of vapor and liquid

References

[1] S. Nukiyama, Maximum and minimum values of heat transmitted from a metal to boiling water under atmospheric pressure, J. Soc. Mech. Eng. (Japan), vol. 37 (1934) 367–374.

[2] G.P. Celata, and Mariani, CHF and post-CHF(post-dryout) heat transfer, Chapter 17, Handbook of phase change, boiling and condensation, edited by Kandlikar, S.G., Shoji, M., and Dhir, V.K., Taylor and Francis, New York (1999) pp. 443-493.

[3] H. Nariai, F. Inasaka, and T. Shimura, Critical heat flux of subcooled flow boiling in narrow tube, proceedings, ASME-JSME Thermal Engineering joint conference, vol. 5 (1987) pp.455-462.

[4] H. Nariai, and F. Inasaka, Critical heat flux and flow characteristics of subcooled flow boiling with water in narrow tubes, Dynamics of two-phase flows, CRC press (1992) pp. 689-708.

[5] S.S. Papell, R.J. Simoneau, and D.D. Brown. Buoyancy effects on critical heat flux of forced convective boiling in vertical flow, NASA TN D-3672 (1965), 17 pages.

[6] A. Bergles, Subcooled burnout on tubes of small diameter, paper No. 63 – WA – 182 ASME (1963).

[7] C.L. Vandervort, A.E. Bergles and M.K. Jensen, An experimental study of critical heat flux in very high heat flux subcooled boiling, Int. J. of Heat and MassTransfer 37(Suppl. 1) (1994) 161–173.

[8] G.P. Celata, Subcooled water flow boiling CHF with very high heat fluxes, Revue Generale De Thermique Fr., ISSN 0035-3159/106/9 (1974) pp. 106-114.

[9] A. Sakurai and M. Shiotsu, Temperature-controlled pool-boiling heat transfer, Proceedings of the fifth International Heat Transfer Conference, vol. 4, B3.1 (1974) pp. 81-85.

[10] F.C. Gunther, Photographic study of surface-boiling heat transfer to water with forced convection, Transactions of the ASME, vol. 73, no. 2 (1951) pp. 115-123.

[11] S.K. Moon, W.P. Baek, and S.H. Chang, Parametric trends analysis of the critical heat flux based on artificial neural networks, Nuclear Engineering and Design, Vol. 163, (1996) pp. 29-49

[12] S.H. Chang, W.P. Baek and T.M. Bae, A study of critical heat flux for low flow of water in vertical round tubes under low pressure, Nuclear Engineering and Design, vol. 132 (1991) pp. 225-237.

[13] S.G: Kandlikar, Critical heat flux in subcooled flow boiling- an assessment of current understanding and future directions for research, Multiphase Science and Technology, vol. 13, no. 3 (2001) pp. 207-232.

[14] S.S. Kutateladze, Heat transfer in condensation and boiling, AEC-tr-3770 (1952), pp.95-113

[15] N. Zuber, Hydrodynamic aspects of boiling heat transfer, AECU-4439, Physics and Mathematics (1959) US Atomic Energy Commission.

[16] J.H. Lienhard and V.K. Dhir, Hydrodynamic prediction of peak pool boiling, Journal of Heat Transfer, Vol.95 (1973) pp.152-158.

[17] H.J. Ivey, D.J. Morris, CHF of saturation and subcooled pool boiling in water at atmospheric pressure, Proceedings of 3rd International Heat Transfer Conference (1966) p. 129

[18] L.S. Tong, Boundary-layer analysis of the flow boiling crisis, Int. J. Heat Mass Transfer 11 (1968) 1208–1211.

[19] W. Hebel, A. Detavernier, and M. Decreton, A contribution to the hydrodynamics of boiling crisis in a forced flow of water, Nuclear Engineering and Design, Vol. 64 (1981) pp. 433-445.

[20] J. Weisman, and B.S. Pei, Prediction of critical heat flux in flow boiling at low qualities, Int. J. of Heat and Mass Transfer, Vol. 26, No. 10 (1983) pp. 1463-1477.

[21] Y. Katto, and Yokoya, Principal mechanism of boiling crisis in pool boiling, Int. J. of Heat and Mass Transfer, Vol. 11 (1970) pp. 993-1002.

[22] Y. Haramura, and Y. Katto, A new hydrodynamic model of critical heat flux, applicable widely to both pool and forced convection boiling on submerged bodies in saturated liquids, Int. J. of Heat and Mass Transfer, Vol. 26 (1983) pp. 379-399.

[23] C. H. Lee, and I, Mudawar, A mechanistic critical heat flux model for subcooled flow boiling based on local bulk flow conditions, Int. J. of Multiphase Flow, Vol. 14, No. 6 (1988,) pp. 711-728.

[24] G.P. Celata, M. Cumo, A. Mariani, M. Simoncini, and G. Zummo, Rationalization of existing mechanistic models for the prediction of water subcooled flow boiling critical heat flux, Int. J. of Heat and Mass Transfer, Vol. 37, Supplement 1 (1994) pp. 347-360.

[25] W. Ding, E. Krepper, U. Hampel, Quantitative prediction of critical heat flux initiation in pool and flow boiling, Int. J. of Thermal Sciences, Vol. 125 (2018) pp 121-131

[26] C.H. Wang and V.K. Dhir, Effect of surface wettability on active nucleation site density during pool boiling of saturated water, J. Heat Transfer, 115 (1993) pp. 659-669

[27] Y. Qi and J.F: Klausner, Heterogeneous nucleation with artificial cavities, J. Heat Transfer, 127 (2005) pp. 1189-1196

[28] Y.H. Zhao, T. Tsuruta and T. Masuoka, Unified theoretical prediction of fully developed nucleate boiling and critical heat flux based on a dynamic microlayer model, Int. J. of Heat and Mass Transfer 45 (2002) 3189-3197.

[29] B.B. Mikic, W.M. Rohsenow, P. Griffith, On bubble growth rates, Int. J. of Heat and Mass Transfer 13 (1970) pp. 657–666.

[30] H Sakashita and A. Ono, Boiling behaviours and critical heat flux on a horizontal plate in saturated pool boiling of water at high pressures, Int. J. of heat and mass transfer, 52, (2009) 744 – 750.

[31] H Sakashita, Critical heat flux on a vertical surface in saturated pool boiling at high pressures Journal of Thermal Science and Technology, Vol. 11, No. 2, (2016).

[32] J.C. Chen, Correlation for boiling heat transfer to saturated fluids in convective flow. Ind. Eng. Chem. Res. 5 (1966) pp. 322–329.

[33] C. Haas, T. Schulenberg and T. Wetzel, Critical heat flux for flow boiling of water at low pressure in vertical internally heated annuli, Int. J. Heat and Mass Transfer 60 (2013) 380-391.

[34] M.S. El-Genk, S. Haynes, S. Kim, Experimental studies of critical heat flux for low flow of water in vertical annuli at near atmospheric pressure, Int. J. Heat and Mass Transfer 31 (1988) 2291–2304.

[35] T. Schoesse, M. Aritomi, Y. Kataoka, S.-R. Lee, Y. Yoshioka, M.K. Chung, Critical heat flux in a vertical annulus under low upward flow near atmospheric pressure, J. Nucl. Sci. Technol. 34 (1997) 559–570.

[36] R. Cole and W.R. Rohsenow, Correlations of bubble departure diameters for boiling of saturated liquids. Chem. Eng. Profr. Symp. Ser. No. 92 (1969) 65 211.

[37] N. I. Kolev, The Influence of mutual bubble interaction on the bubble departure diameter. Experimental Thermal and Fluid Science 8 (1994) pp. 167–174.

[38] R.M. Sugrue, The effects of orientation angle, subcooling, heat flux, mass flux, and pressure on bubble growth and detachment in subcooled flow boiling, Master Thesis in Nuclear Science and Engineering, Massachusetts Institute of Technology, Cambridge, MA, 2012

[39] F. Fischer, D. Hoppe, E. Schleicher, G. Mattausch, H. Flaske, R. Bartel, U Hampel, An ultra fast electron beam x-ray tomography scanner. Meas Sci Technol. 19(9) (2008) :094002 DOI: 10.1088/0957-0233/19/9/094002.

[40] F. Barthel, R. Franz, and U. Hampel, Experimental investigations of single and two-phase flow in a heated rod bundle. Kerntechnik Vol. 78, No. 1 (2013) pp. 60-67.

[41] K. Lee, S Baik, T Ro, An utilization of liquid sublayer dryout mechanism in predicting critical eat flux under low pressure and low velocity conditions in round tubes. Nuclear Engineering and Design 200 (2000) pp 69-81.